Biomedicine & Pharmacotherapy 137 (2021) 111357

Contents lists available at ScienceDirect

Biomedicine & Pharmacotherapy

journal homepage: www.elsevier.com/locate/biopha

Original article

Therapeutic efficacy of 3,4-Diaminopyridine phosphate on neuromuscular junction in Pompe disease

Bragato Cinzia [a,*], Blasevich Flavia [a], Ingenito Gary [b], Mantegazza Renato [a], Maggi Lorenzo [a]

[a] Neuromuscular Diseases and Neuroimmunology Unit, Fondazione IRCCS Istituto Neurologico Carlo Besta, Via Celoria 11, Milan 20133, Italy
[b] Catalyst Pharmaceuticals Inc, Coral Gables, FL, USA

ARTICLE INFO

Keywords:
Pompe disease
Acid α-glucosidase
3,4-Diaminopyridine phosphate (3,4-DAPP)
Zebrafish
Neuromuscular junction (NMJ)

ABSTRACT

3,4-Diaminopyridine (3,4-DAP) and its phosphate form, 3,4-DAPP have been used efficiently in the past years to treat muscular weakness in myasthenic syndromes with neuromuscular junctions (NMJs) impairment. Pompe disease (PD), an autosomal recessive metabolic disorder due to a defect of the lysosomal enzyme α-glucosidase (GAA), presents some secondary symptoms that are related to neuromuscular transmission dysfunction, resulting in endurance and strength failure. In order to evaluate whether 3,4-DAPP could have a beneficial effect on this pathology, we took advantage of a transient zebrafish PD model that we previously generated and characterized. We investigated presynaptic and postsynaptic structures, NMJs at the electron microscopy level, and zebrafish behavior, before and after treatment with 3,4-DAPP. After drug administration, we observed an increase in the number of acetylcholine receptors an increment in the percentage of NMJs with normal structure and amelioration in embryo behavior, with recovery of typical movements that were lost in the embryo PD model. Our results revealed early NMJ impairment in Pompe zebrafish model with improvement after administration of 3,4-DAPP, suggesting its potential use as symptomatic drug in patients with Pompe disease.

1. Introduction

Glycogenosis type II (glycogen storage disease type II; OMIM #232300) is a multisystemic disorder described for the first time in 1932 by the Dutch pathologist Johannes Cassianus Pompe. This pathology, later named Pompe disease (PD), is an autosomal recessive disorder caused by mutations in the gene coding for the acid alpha-glucosidase (GAA) enzyme responsible for breaking down glycogen.

The spectrum of the disease severity encompasses a broad continuum of phenotypes, going from the severe "classic" form, characterized by childhood-onset, severe cardiomyopathy, rapidly progressive course and fatal outcome before two years of age, to the "intermediate" infantile form characterized by milder phenotype, to the juvenile and adult forms characterized by prevalent involvement of skeletal muscle with frequent respiratory insufficiency. The extent of residual enzyme activity generally correlates with disease severity [1–4].

The enzyme replacement therapy (ERT), with the GAA provided via intravenous infusion, is the only therapy available since 2006, representing a major milestone in the treatment of PD. The ERT was found to be most efficacious in the infantile severe form, while not all late onset cases respond equally well to this treatment [1,3,5,6]. Therefore, the correction of the skeletal muscle phenotype in late onset cases is still challenging, revealing a need for more effective therapies [7–9].

Neuromuscular junction (NMJ) function and structure impairment has been described in the *gaa* knockout mouse model with both pre- and postsynaptic pathology, rescued by GAA gene therapy. NMJ involvement may contribute to the PD phenotype, in particular to the fatigue complained by patients with LOPD (late-onset PD) during daily activities [10–13].

Primary NMJ diseases include Myasthenia gravis, Lambert–Eaton myasthenic syndrome (LEMS), neuromyotonia and congenital myasthenic syndromes; however, NMJ impairment has been also observed in spinal muscular atrophy (SMA), Charcot–Marie–Tooth (CMT), amyotrophic lateral sclerosis (ALS) and myotubular/centronuclear myopathy [14].

Taking advantage of the drug repurposing strategy, aimed at identifying new uses of already approved drugs, and of the zebrafish PD animal model [15], we proposed to use the Amifampridine phosphate, also called 3,4-Diaminopyridine phosphate (3,4-DAPP) or Firdapse, to address the NMJ dysfunction in PD patients. 3,4-DAPP is the only

* Correspondence to: Muscle Cell Biology Lab, Fondazione IRCCS Istituto Neurologico Carlo Besta, Via Amadeo 42, 20133 Milano, Italy.
E-mail address: cinzia.bragato@istituto-besta.it (B. Cinzia).

https://doi.org/10.1016/j.biopha.2021.111357
Received 4 December 2020; Received in revised form 25 January 2021; Accepted 31 January 2021
Available online 19 February 2021

approved therapy for adult patients with LEMS by the Food and Drug Administration (FDA) and by the European Medicines Agency (EMA), and is also recognized as an orphan drug (see Orphanet definitions of orphan drugs at: https://www.orpha.net/consor/cgi-bin/Education_AboutOrphanDrugs.php?lng=EN) for the treatment of patients with myasthenia gravis [16–18].

The principal effect of 3,4-DAPP is to block potassium channels in nerve terminals at the presynaptic level of the NMJ, resulting in a prolonged action potential and a longer depolarization. As a result of this protracted depolarization, the voltage-gated calcium channels remain open longer than usual and increase the entry of calcium into the nerve terminal, facilitating membrane fusion events and thus leading to increased acetylcholine (ACh) discharge from motor neuron presynaptic terminal [19]. This neurotransmitter diffuses across the synaptic cleft and binds acetylcholine receptors (AChRs), a key molecular component positioned at the postsynaptic muscle membrane. The binding of ACh to AChRs is responsible for the generation of the endplate potential (EPP) which, exceeding the threshold potential necessary to activate voltage-gated sodium channels, triggers a muscle action potential, causing muscle contraction [20].

Zebrafish (*Danio rerio*) has been used as a model for drug discovery since the beginning of the twenty-first century and has successively become an attractive tool even for drug repurposing. Drug administration is simplified in this model being achieved through the aqueous environment, and the efficacy, bioavailability and toxicity can be readily determined. Moreover, the embryos are easy to handle and can be genetically manipulated by morpholino antisense oligonucleotide, mRNAs, transgenes, and genome editing techniques such as Clustered Regularly Interspersed Palindromic Repeats (CRISPR)-Cas9, Transcription Activator-Like Nucleases (TALENs), and Zinc Finger Nucleases (ZFNs) [21,22].

In a previous work, we have characterized a knockdown zebrafish Pompe disease model, generated by transiently knocking down *gaa* expression using antisense morpholino oligonucleotides (MO) [15]. Our zebrafish transient model of PD shows several pathological characteristics recapitulating PD features, especially evident in embryos injected with a MO targeting the splice site between intron 9 and exon 10, close to the catalytic site of the Gaa protein (I9E10*gaa*-MO). Accumulation of glycogen content within the muscle fiber, the most known hallmark of PD, was noted in embryos injected with this specific MO (morphants); in addition, markedly altered motor behavior and altered expression of autophagy-related transcripts and proteins were observed. In this context, our zebrafish Pompe disease model is an amenable tool for investigating the effects of 3,4-DAPP as a drug with potential therapeutic efficacy in PD.

In the present study, we assessed efficacy of 3,4-DAPP treatment on both neuromuscular junction (NMJ) morphology and muscle performance in zebrafish PD embryos, by investigating neuromuscular junction structure at the optical and electron microscopy level, and motor behavior by quantification of spontaneous coiling activity and touch evoked motility test.

2. Materials and methods

2.1. Animal care

Zebrafish were raised and maintained at the University of Milan facility.

The study was approved by the animal ethics committee of the University and carried out at the University of Milan facility. Animals were injected according to the principles of Good Animal Practice as defined by Italian animal welfare regulations. All experiments were performed on embryos and larvae (AB strain) within 5 days post fertilization (dpf), thus not subject to animal experimentation rules according to European and Italian directives.

2.2. Embryo maintenance

The adult fish were maintained at 28 °C on a 14 h light/10 h dark cycle and mated in order to collect the embryos to be used. The embryos collected were staged according to Kimmel et al. [23]. For the whole-mount immunofluorescence experiments, the embryos were raised in 0.003% 1-phenyl-2 thiourea (Sigma-Aldrich) to avoid pigmentation.

2.3. Morpholino injections

Characterization of the zebrafish PD model (including use of different morpholinos and variable concentrations, concentration chosen for experimental procedures, variability of phenotypes obtained, etc.) is reported in Bragato et al. [15]. For the present study, zebrafish gaa was knocked down by the use of a splicing morpholino oligonucleotide, called I9E10*gaa*-MO (5′-tgtgattttcttgtttacagGACAT-3′), directed against the splice site present between intron 9 and exon 10, close to the region encoding the catalytic site of the Gaa protein [15].

After timed mating of adult zebrafish, fertilized eggs were collected and injected at the 1 or 2-cell stage using an Eppendorf TransferMan NK2 micromanipulator (Eppendorf). Embryos were injected with either I9E10*gaa*-MO (1 pmol/embryo) and standard control morpholino at the same concentration (to verify the absence of morpholino-mediated toxicity) in a volume of 4 nl.

Morpholinos were diluted in Danieau's solution [24]. Phenol Red was co-injected as tracer to enable monitoring with a stereomicroscope Leica MZ FLIII.

Embryos injected with morpholino (morphants) were then allowed to develop in fish water at 28 °C up to the stage of interest.

2.4. 3,4-DAPP treatments

A range of concentrations of 3,4-DAPP, starting from 20 micromolar (μM) to 2 mM, was tested in embryos at 60% of epiboly stage and an increase in myoclonus movements (brief involuntary movements) was observed in a dose dependent manner. The 3,4-DAPP concentration to be used was chosen by analyzing spontaneous movements in I9E10*gaa*-MO injected embryos that, after drug treatment, had to be similar to STD-Ctrl embryos (Supplementary Fig. 1).

3,4-DAPP was diluted in 20 ml of fish water at the chosen concentration, administered to chorion deprived embryos, and replaced freshly every day till the required experimental stage.

Chorion deprivation was obtained in order to avoid a possible protection by the chorion itself, by the use of Pronase E (EC 3.4.24.4) from Sigma–Aldrich (Germany).

2.5. AChR labeling

Morphants at the stage of 48 h post fertilization were fixed in 4% para-formaldehyde solution (PFA) and α-bungarotoxin (α-BTX) labeling was performed.

For this experiment 32 standard control embryos, 30 untreated I9E10*gaa*-MO embryos and 31 I9E10*gaa*-MO embryos treated with 50 μM 3,4-DAPP, were used.

Morphants were incubated for 30 min at room temperature in 10 g/ml Rhodamine-conjugated α-BTX (Sigma-Aldrich, Saint Louis, MO, USA), diluted in BSA-PBS-Triton (5% normal bovine serum, and 1% Tween in PBS-Triton), washed in PBS-Triton, mounted in glycerol and observed under a Leica confocal microscope equipped with hybrid and argon lasers (Leica Microsystems, Wetzlar, Germany).

For acquisition, the tail of 48 hpf embryo (about 20 μm thick), was divided into 25 frames, covering a 0.8 μm area in z. The maximum projection was generated successively using 5 frames, starting from the frame number 1 to number 5, and from the left side of the embryo.

To quantify the α-BTX level, the red signal area was calculated on

each confocal z-stack by means of Fiji software version 2.0 (http://rsb.info.nih.gov/nih-image/) on micrographs taken at the same exposure conditions [25].

2.6. Myofiber cultures

Myofiber preparations from 3 dpf larvae were obtained as previously described [26]. Briefly, larvae were dissociated in 10 mM collagenase type I (Sigma) for 90 min at RT. Larvae were triturated every 30 min. Dissociated preparations were re-suspended in CO_2-independent media (Gibco), passed through a 40 mm filter (Falcon), and plated onto glass coverslips pre-coated with poly-L-lysine (Sigma). Cells were stained using α-bungarotoxin (Invitrogen, 1:100 in PBST), which binds to the nicotinic acetylcholine receptor at the postsynaptic side of NMJs, and Alexa-Fluor 488 phalloidin (1:10; Life Technologies), which binds to all variants of actin filaments, for 40 min. Phalloidin, a highly selective bicyclic peptide, was used to determine the myofiber morphology.

2.7. Immunohistochemistry

All antibodies were diluted in blocking solution (5% w/v bovine serum albumin [BSA] in phosphate buffered saline [PBS] plus 0.1% Tween20).

After 2 h fixation in 4% PFA at room temperature (RT), embryos were washed 5 times for 5 min in 0.1% PBS-Tween, rinsed in water, permeabilized for 7 min in cold acetone, rinsed in water, washed 5 times for 5 min in 0.1% PBS-Tween, incubated in NH4Cl solution for 30 min at room temperature, blocked for 3 h at room temperature in blocking solution and then incubated overnight at 4 °C with primary antibody directed against the synaptic vesicle glycoprotein 2 A (SV2A). The second day, embryos were washed 5 times for 10 min in 0.1% PBS-Tween, then every 2–3 h with blocking solution at RT on a shaker until incubation in the secondary antibody overnight at 4 °C. The third day embryos were washed 3 times for 5 min in 0.1% PBS-Tween at RT.

Mouse anti-synaptic vesicle glycoprotein 2A (SV2A) recognizing all the three isoforms: SV2A, SV2B and SV2C (DSHB, Developmental Studies Hybridoma Bank, Iowa City, Iowa, USA), diluted 1:200, was used.

As secondary antibody, Alexa 488-conjugated goat anti-mouse IgG (Invitrogen Life Technologies, Carlsbad, CA, USA) diluted 1:1000, was used.

The labeling of AChRs with α-bungarotoxin was previously described [27]. Briefly, after incubation with primary and secondary antibody, embryos were incubated for 30 min at room temperature in 10 g/ml Alexa 547-conjugated α-BTX (Sigma-Aldrich, Saint Louis, MO, USA) diluted in BSA-PBS-Triton (5% normal bovine serum, and 1% Tween in PBS-Triton), washed in PBS-Triton, and mounted in glycerol.

2.8. Morphological characterization of embryo NMJ ultrastructure

In order to observe subtle neuromuscular junction changes, embryos were fixed, dehydrated, embedded in resin and thin sectioned for electron microscopy examination. Briefly, zebrafish at 4 dpf were fixed 2 h in 2.5% glutaraldehyde in sodium phosphate buffer, pH 7.4; left in buffer overnight at 4 °C; post-fixed 1 h in 2% phosphate-buffered OsO4, dehydrated in graded ethanol, and embedded in epoxy resins (Electron Microscopy Sciences, Hatfield, Pennsylvania). Ultrathin sections (70 nm thick) of zebrafish tails were collected onto grids, stained with uranyl-less (Electron Microscopy Sciences) and Reynolds solution, and examined with a FEI Tecnai G2 Spirit electron microscope (FEI Hillsboro, Oregon, United States).

2.9. Spontaneous tail coiling analyses

Spontaneous tail coiling behavior was evaluated in morphants either treated with 3,4-DAPP or untreated, and in controls, at 24 hpf. Embryos were chorion deprived, anesthetized with Tricaine (3-amino benzoic acid ethyl ester) (Sigma; A-5040) suspended in fish water (without 3,4-DAPP), and transferred to a 3.5 mm round petri dish with glass bottom. After transferring embryos, the Tricaine was replaced with 1.5% low-melting-point agarose in fish water at 37 °C. Embryos were then oriented with the dorsal side up. Once the agarose solidified, the tail was gently cleared from agarose and a drop of fish water was added on the top of the fish.

Spontaneous tail coiling was then recorded during a 30 s time frame (time resolution 250 frames/μs) using a digital camera (Olympus) mounted on a stereomicroscope (Leica Microsystems). For each embryo, a video record of the frequency of spontaneous tail coiling, the percentage of coilings, which consist of two or more repeated bends of the trunk before returning to the resting position, the relative number of contralateral left-right bends or ipsilateral bends, and the angle of maximum amplitude of tail flexion, was made [28].

2.10. Screening for embryonic motility

Embryos at 3 dpf, either STD-Ctrl (hereinafter called control embryos), or I9E10*gaa*-MO untreated (hereinafter called morphants) or I9E10*gaa*-MO treated with 50 μM 3,4-DAPP (hereinafter called 3,4-DAPP treated morphants), were subjected to tactile stimulation using a micro-loader. A gentle impulse was applied to the tail of the embryo and the reaction was observed (touch-evoked motility test) [29]. Upon application of the tactile stimulus STD-Ctrl larvae normally swim away from the source of the impulse, while embryos injected with morpholino oligonucleotides (morphants) show variably reduced motility, and morphants treated show an increase in escape behavior.

The results were obtained by observing the embryos under a stereomicroscope equipped with a Leica DCF 480 digital camera and IM50 software (Leica).

2.11. Data analysis

In all experiments, morphants were compared to embryos at the same developmental stage, injected with the same amount of a control standard morpholino (controls). A one-way ANOVA statistical analysis was conducted between morphants, 3,4-DAPP treated morphants and controls to compare the effects of the 3,4-DAPP treatment. Post hoc comparison using the Tukey HSD test was reported. Results were expressed as means (M) and standard deviation (SD). Chi-square test was used to compare embryos movements, when appropriate. P values were considered significant: $*p \leq 0.05$, $**p \leq 0.01$; $***p \leq 0.001$. For graphs GraphPad Prism software was used, while for figures Adobe Photoshop was used.

2.12. Quantitation

In order to quantify the α-bungarotoxin (α-BTX) signal level, the red area expressed as arbitrary units was calculated on each confocal z-stack by the use of Fiji software version 2.0 (http://rsb.info.nih.gov/nih-image/) on micrographs taken at same exposure conditions [26]. Briefly, fields occupied by the entire tail of the animal were photographed from each z-stack and digitalized. Using the software, a threshold was applied to the photographs to obtain red and black images with areas positive for α–BTX in red and negative areas in black. The area positive for α-BTX was calculated as a percentage of the entire image on each confocal z-stack, and the mean percentage calculated. The same procedure was repeated for each group of animals, and the mean percentage calculated (see Bragato et al. [30]).

Myofibers were analyzed on micrographs taken at 40X under a Zeiss Axioplan2 microscope. The α-BTX signal level was evaluated as described above. Determination of myofibers length was obtained using Microscope Software AxioVision Release 4.8.2 (Zeiss, Oberkochen, Germany).

Quantification of SV2A/α-BTX co-localization signal was obtained using the Fiji plugin JaCoP (Just another Colocalization Plugin) analysis [31]. SV2 was imaged with the 488-green channel, (488 nm laser and emission between 495 and 519 nm), and α–BTX with the 561-red channel (556 nm laser and emission between 573 and 600 nm). We used an internal feature of Leica analysis software to avoid saturation condition. The measurement of SV2A overlapping with α-BTX, was calculated on the entire field of images obtained by 5 confocal z-stacks of the tail of embryos from each experimental group. Thresholds were automatically calculated by the software and not set by the operator to avoid biased data. The co-localization measures were reported as Pearson's r^2 units, and comparisons between the three groups were done by 1way-ANOVA with post hoc Tukey HDS analysis.

3. Results

3.1. I9E10gaa-morpholino injected embryos displayed phenotypic defects recapitulating Pompe disease defects

In order to obtain the zebrafish PD transient model which better recapitulates the disease features, the I9E10*gaa*-morpholino, at a concentration of 1 pmol/embryo, previously characterized in Bragato et al. [15] was used.

The morphants were divided into C1 to C3 phenotypic classes, [16] and the morphants pertaining to the C1 and C2 classes were used for the experiments.

The characteristics of morphants referred to C1 class, were: normal-appearing morphology and completely formed somites; the traits of morphants pertaining to C2 class were: partially disrupted somites and features such as cardiac edema, enlargement of the IV cerebral ventricle or both alterations; while C3class included morphants with unformed or totally disrupted somites [15].

For each experiment, morphants were compared to embryos injected with a scrambled morpholino (controls) at the same developmental stage.

3.2. 3,4-DAPP administration improved correct acetylcholine receptors cluster localization

Morphants were treated with a concentration of 50 μM 3,4-DAPP, starting from the stage of 60% of epiboly, prior to the neuromuscular junctions' formation, which takes place around the 24 hpf developmental stage.

At 48 hpf, injected embryos pertaining to C1 class were stained with α-BTX, and evaluated under a confocal microscope. The four somites located immediately after the end of the yolk were chosen for this analysis (Fig. 1A and B).

There was a significant modification of α-BTX signal at the $p < 0.05$ level for the three conditions [$F(2, 18) = 11.78$, $p = 0.0005$].

Post hoc using the Tukey HSD test indicated that the mean score for the α-BTX signal in morphants ($M = 2129$, $SD = 416.6$) was significantly different compared to α-BTX signal both in control embryos ($M = 7904$, $SD = 3216$) and in 3,4-DAPP treated morphants ($M = 4818$, $SD = 1601$).

However, the α-BTX signal in 3,4-DAPP treated morphants showed no significant change when compared to controls.

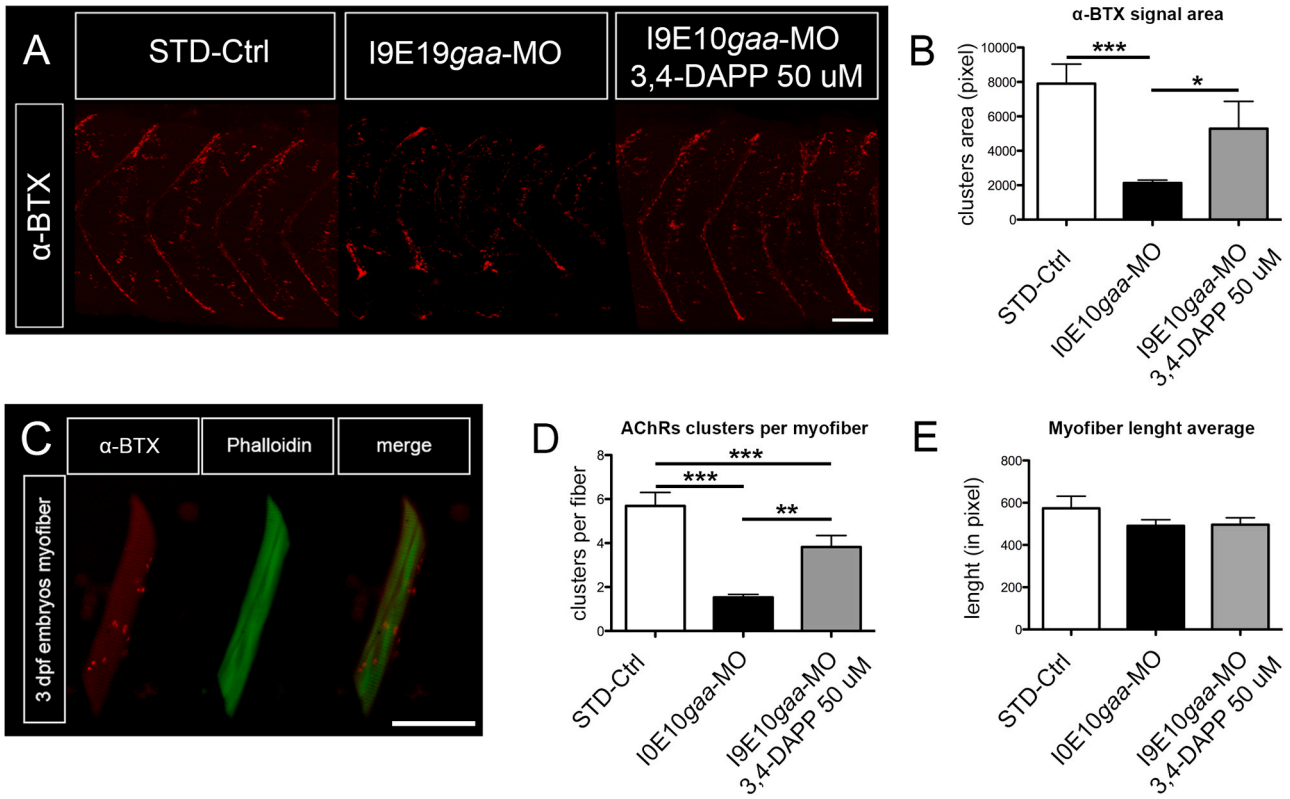

Fig. 1. 3,4-DAPP administration increased density and appropriate spatial positioning of AChRs. (A) Representative image of AChRs (α-BTX) in 4 somites of zebrafish embryos at 48 hpf collected during 3 distinct experiments. STD-Ctrl embryos: n = 32, untreated I9E10*gaa*-MO: n = 30, and I9E10*gaa*-MO treated with 3,4-DAPP 50 μM: n = 31, Scale bar = 25 μm. (B) Quantification of α-BTX-positive spots in the three experimental groups. (C) Representative image of single myofibers obtained after dissociation from 3 dpf embryos. Scale bar = 30 μm. (D,E) Quantification of AChR clusters in dissociated myofibers (D), and of myofiber average length (E) in the three experimental groups. Note that myofiber average lengths are comparable. Error bars in (B), (D), (E) are SEMs.

3.3. Single myofibers presented an increased number of acetylcholine receptor clusters after 3,4-DAPP administration

To support the results obtained by the α-BTX labelling experiment on whole-mount embryos, single myofibers were evaluated.

Myofibers from 3 dpf larvae pertaining to the three experimental groups, were dissociated and labelled with α-BTX and Alexa-Fluor 488 phalloidin (Fig. 1C–E).

Also in this case we observed significant differences among the three experimental conditions [$F(2, 51) = 25.43$, $p < 0.0001$].

In particular, increased numbers of acetylcholine receptor (AChR) clusters were observed in myofibers pertaining to 3,4-DAPP treated morphants ($M = 2.858$, $SD = 1.671$), compared myofibers of untreated morphants' ($M = 1.467$, $SD = 0.4492$).

Myofibers from both treated and untreated morphants, showed a significant decrease in AChR clusters compared to control embryos ($M = 7.411$, $SD = 4.187$).

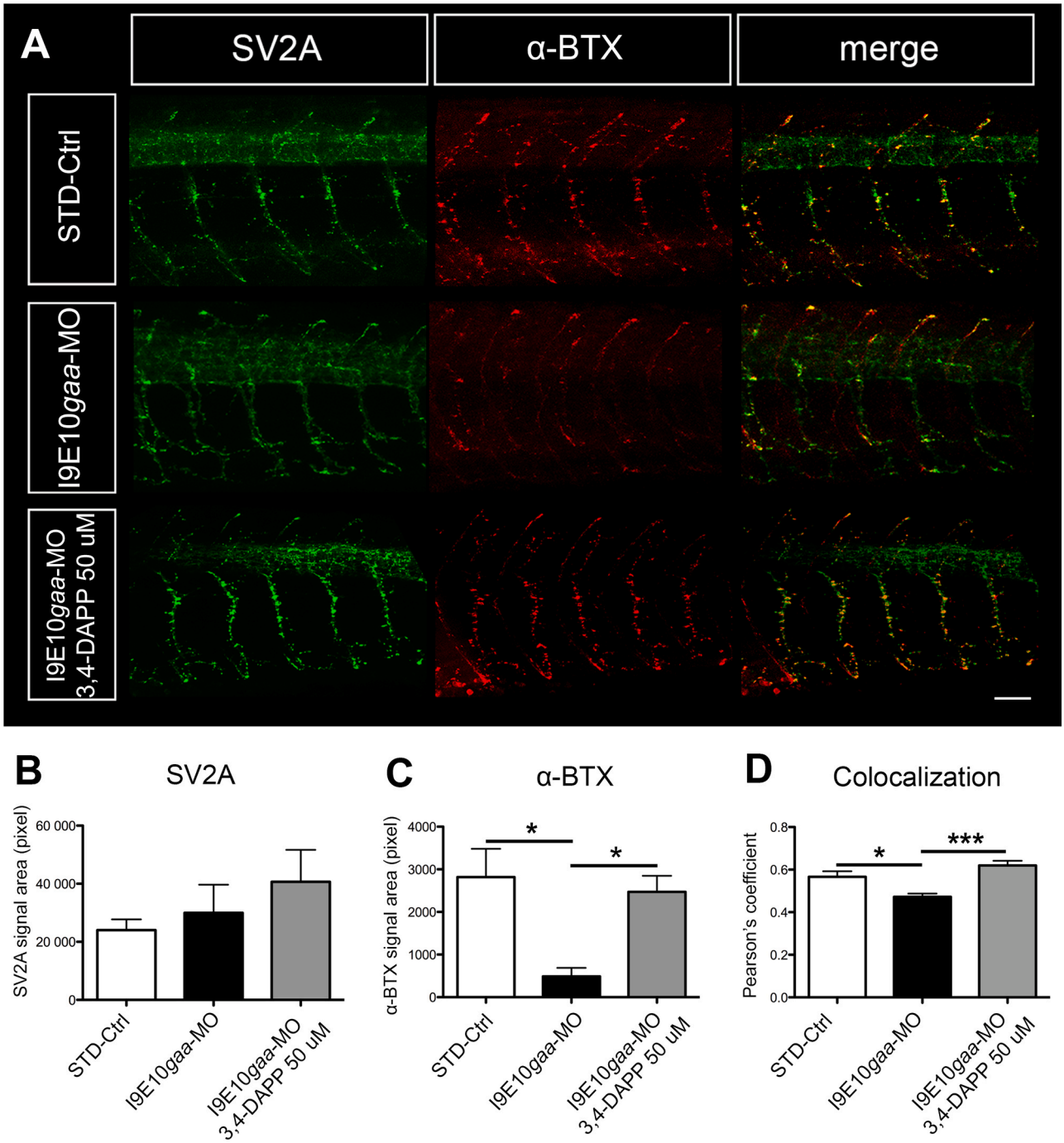

Fig. 2. 3,4-Diaminopyridine phosphate administration increased pre- and postsynaptic signal co-localization. (A) Representative confocal fluorescence maximum projection images of SV2A (green) and α-BTX (red) signal in 5 spinal hemisegments and somites in embryos at 48 hpf. The images are representative of those found in $n = 10$ embryos for each experimental group (controls, morphants and 3,4-DAP treated morphants), during 3 distinct experiments. Scale bar = 25 μm. (B–D) Quantification of the SV2A (B) green signal, the α-BTX (C) red signal, and the co-localization signal (D). Error bars are SEMs. (For interpretation of the references to colour in this figure legend, the reader is referred to the web version of this article.)

3.4. 3,4-DAPP administration showed effects on co-localization of pre- and postsynaptic elements

Anti-SV2A antibody and fluorescent α-BTX staining were used to analyze pre- and postsynaptic elements in 15 embryos for each group (controls, morphants and 3,4-DAPP treated morphants) at 48 hpf, collected during 3 different experiments (Fig. 2A).

The presynaptic SV2A signal was not significantly increased in 3,4-DAPP treated morphants compared to both morphants and control embryos, nor it was in morphants, compared to control embryos (Fig. 2B).

However, when the postsynaptic α-BTX signal was analyzed, different results were obtained confirming the data achieved in the previous experiments [$F(2,9) = 7.612$, $p = 0.0116$]. Untreated morphants ($M = 488.8$, $SD = 396.4$) showed a significant decrease in the α-BTX signal compared to both, 3,4-DAPP treated morphants ($M = 2470$, $SD = 756.4$) and controls ($M = 2819$, $SD = 1327$). In particular, the 3,4-DAPP treated morphants showed an α-BTX signal comparable to that of the control embryos (Fig. 2C).

When the pre- and postsynaptic signals were analyzed in terms of co-localization [$F(2,12) = 10.3$, $p = 0.0025$], a significantly higher co-localization of SV2A and α-BTX signals was observed in 3,4-DAPP treated morphants ($M=0.6198$, $SD = 0.04430$) compared to untreated morphants ($M = 0.4726$, $SD = 0.03387$); a significantly lower in SV2A and α-BTX co-localization signal was observed in untreated morphants compared to control embryos ($M = 0.5667$, $SD = 0.06208$); while no significant differences were observed between 3,4-DAPP treated morphants and controls (Fig. 2D).

Motor axon length, number of axonal branches, and distance between the site from which the axon leaves the spinal cord and the first branching point were analyzed on the three experimental groups. Results obtained from these analyses, performed on confocal maximum projections fluorescence images of 3,4-DAPP treated morphants, morphants and control embryos, failed to show any significant difference.

3.5. 3,4-DAPP improved neuromuscular junctions' ultrastructure in I9E10gaa-morphants

Electron microscopy analysis was carried out on morphants ($n = 12$), 3,4-DAPP treated morphants ($n = 10$) and control embryos ($n = 10$), collected during 3 experiments.

Untreated morphants showed NMJs with enlarged swollen presynaptic terminals and a convoluted appearance in 46% of the observed neuromuscular junctions, compared to both, 3,4-DAPP treated morphants, in which only 15% of the NMJ structure appeared altered, and control embryos, in which none of the NMJs showed morphological defects (Fig. 3A).

Since 3,4-Diaminopyridine blocks potassium channels in nerve terminals, causing increase in acetylcholine release, the number of acetylcholine vesicles was assessed [$F(2,27) = 10.96$, $p = 0.0003$]. NMJs of untreated morphants ($M = 25.10$, $SD = 14.36$) were characterized by a significant decrease in acetylcholine vesicle numbers compared to both, 3,4-DAPP treated morphants ($M = 83.10$, $SD = 28.14$) and control embryos ($M = 61.10$, $SD = 36.71$) (Fig. 3B). Comparison between 3,4-DAPP treated morphants, and control embryos, failed to show any significant difference, although acetylcholine vesicles present in NMJs of 3,4-DAPP treated morphants were 30% more of than vesicles present in control NMJs (Fig. 3C).

3.6. Behavioral analyses showed improvement after 3,4-DAPP treatment

The spontaneous coiling of morphants, was assessed in the three

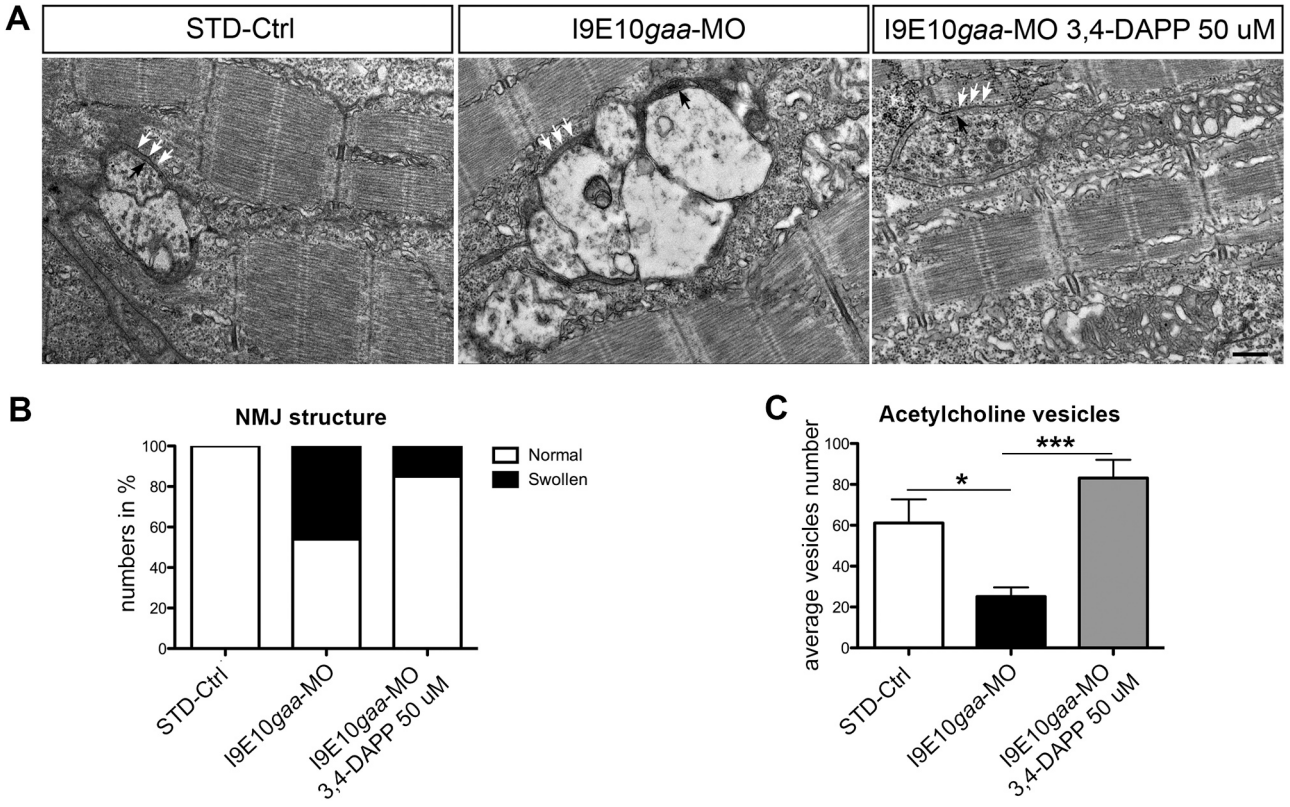

Fig. 3. 3,4-Diaminopyridine phosphate improved NMJs in zebrafish embryos. (A) Electron micrographs showing a swollen and convoluted end-plate in a morphant, a normal appearing end-plate in a 3,4-DAPP treated morphant and a normal endplate in a control embryo. Note the synaptic cleft (white arrows) and active zones (black arrows). Scale bar = 2 μm. (B,C) Quantification of the percentage of NMJs presenting normal structure (B), and of acetylcholine vesicles (C), in the three experimental groups. Error bars are SEMs.

experimental groups at 24 hpf [F(2,24) = 395.6, p < 0.0001] (Fig. 4).

In control embryos (M = 81.00, SD = 2.872) (Fig. 4A) the tail reached almost 90° of maximum angle of flexion during spontaneous movements, while in morphants (M = 42.44, SD = 3.609) (Fig. 4B), the maximum degrees of flexion reached by the tail was significantly decreased (Fig. 4C).

After 3,4-DAPP administration (M = 82.33, SD = 3.708), the tail flexion was similar to controls, and significantly increased compared to untreated morphants.

Furthermore, 44% of the untreated morphants showed lack of spontaneous coiling, compared to 29% of 3,4-DAPP treated morphants and to 22% of control embryos (p = 0.0029, Chi-Square test) (Fig. 4D).

Evaluation of the type of coiling [F(2,24) = 3.792, p = 0.0371], by means of ipsilateral or left-side contralateral tail movement, showed a decrease in ipsilateral coiling in untreated morphants (M = 2.333, SD = 2.345), compared to 3,4-DAPP treated morphants (M = 6.222, SD = 2.682) and to control embryos (M = 4.889, SD = 3.887). The number of contralateral tail coiling was similar in the three experimental groups (Fig. 4E).

The touch evoked response test, performed in morphants, in 3,4-DAPP treated morphants and control embryos at 3 dpf, showed that, in comparison to control embryos, a slight escape attempt was present in 7 out of 30 untreated morphants, as well as a very weak escape contraction and muscle stiffness. After treatment with 50 μM 3,4-DAPP, the number of embryos presenting an improvement in escape contractions increased to 24 out of 30 morphants (Supplementary Fig. 2).

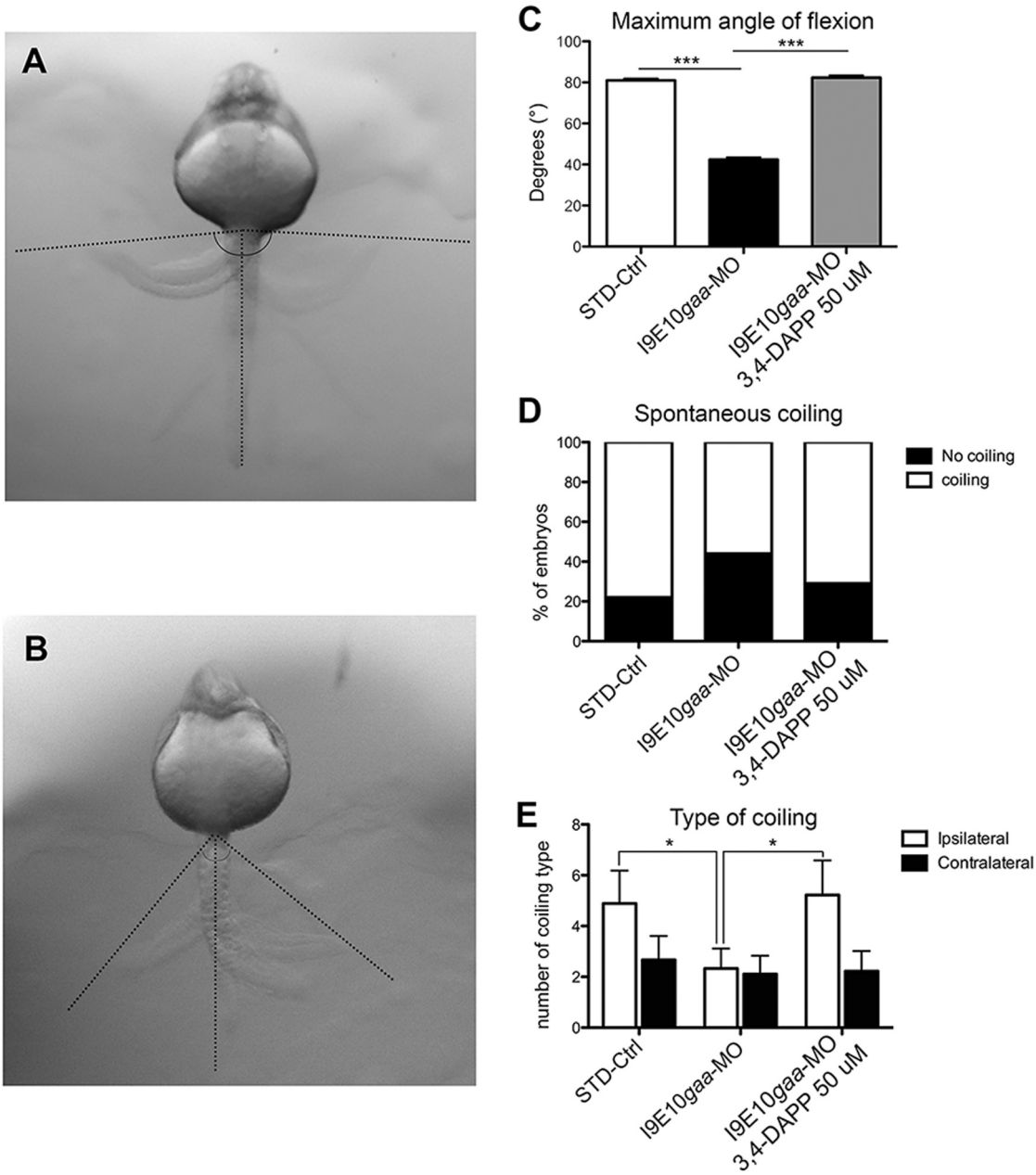

Fig. 4. I9E10*gaa*-MO injected embryos behavior is ameliorated by 3,4-DAPP administration. (A, B) Representative images of 3,4-DAPP treated morphants (A), and untreated morphants (B) showing the maximum angle of flexion reached by the tail, during spontaneous tail coiling behavior at 24 hpf. (C–E) Quantification of the maximum angle of tail flexion (C), percentage of morphants showing spontaneous movements (D), and number of ipsilateral and contralateral bends of the entire body, recorded during a 30 s' time-frame (E), in the three experimental groups. Error bars are SEMs.

4. Discussion and conclusion

The drug repurposing strategy offers many advantages over completely developing a novel drug for a given medical suggestion. The risk of failure is lower, in particular from a safety standpoint. Furthermore, the drug development time can be reduced, less investment is needed and, potentially, patients would benefit sooner from a repurposed medicine [32].

Different pathologies are often presenting similar defects that hypothetically can be improved by known drugs. We pointed out amifampridine (3,4-Diaminopyridine phosphate) as a possible symptomatic treatment to be used in PD.

3,4-Diaminopyridine phosphate has been reported to be useful in the treatment of diseases that are characterized by neuromuscular junction impairment (NMJ), such as Lambert-Eaton myasthenic syndromes and Congenital Myasthenic syndromes and more recently Myasthenia gravis and other pathologies in humans [14,33–35].

In this regard, NMJ alterations in PD may be considered as contributors to the disease phenotype and progression [13]. Such changes are probably uncorrectable by ERT administration to muscle, as muscle glycogen normalization by ERT would be ineffective in restoring motor endplate function, particularly in later stages of the disease. Therefore, we envisaged that a possible improvement of the NMJ function by 3, 4-DAPP would ameliorate fatigue and motor function in PD patients.

Even though ERT has been shown to be efficacious in the treatment of infantile patients, there is a huge unmet medical need to ameliorate the skeletal muscle condition in late onset Pompe disease patients, which are much less responsive to this treatment with relevant disabilities [7–9,36].

In our previous paper, we demonstrated that the zebrafish PD model is a suitable, rapid and low cost tool both for investigating pathogenic mechanisms of the disease and for testing compounds with therapeutic potential. We now confirm our previous assumptions and demonstrate that indeed the zebrafish PD model recapitulates most aspects of the disease found in humans, including defects of the NMJ, and that the model is useful to test a compound such as 3,4-DAPP.

We were able to detect NMJ abnormalities by two different methods using α-BTX to determine AChRs clusters in whole-mount embryos and in dissociated myofibers and by measuring co-localization of a presynaptic marker with α-BTX. This was further confirmed by ultrastructural analysis of the end plates, which showed an increase in abnormally swollen motor nerve terminals and significant decrease in acetylcholine vesicle numbers in NMJ of *gaa* morphants. By confocal microscopy at 48 hpf, we observed a conserved conformation of presynaptic structures (i.e. number and conformation of terminal branching), while the post-synaptic structures, as expected, were altered, and changes were appreciable even by confocal microscopy. We believe that post-synaptic changes are more severe and, therefore, evident at earlier stages and with less sensible morphological methods, while presynaptic changes are subtler and perceptible only at later stages (i.e. at 4 dpf) and with more sensible methods such as electron microscopy.

The reason why, in the present work, we performed confocal microscopy analysis in embryos at 48 h post fertilization, and electron microscopy in 4 day-old embryos, was due to the fact that acceptable immunohistochemistry results by confocal microscopy would not be obtainable in 4 day-old embryos, based on the intricate pattern of motorneurons that are present at this stage. On the other end, ultrastructural studies had to be performed in 4 day-old embryos in order to have a complete development of the pathological condition in the skeletal muscle system.

All our experiments showed that 3,4-DAPP treatment improved NMJ abnormalities including number and localization of AChR clusters, NMJ ultrastructural morphology and number of ACh presynaptic vesicles.

Finally, the analysis of motor behavior showed in embryos at 24 hpf an increase in angle flexion of the tail and in spontaneous coiling movements after treatment with 3,4-DAPP. We monitored in particular this developmental stage because it is a transient period of alternating spontaneous tail coiling, which starts at 17 h post fertilization, and can be modified by exposure to a wide range of diverse chemicals and because the analysis of spontaneous coiling movement has the potential to discriminate neurotoxic activity [37]; while, later in time, there is a progressive refinement of locomotor network circuits during the development, leading to the establishment of organized swimming by 96 hpf [28].

Taken together, our results confirmed that the use of 3,4-DAPP effectively rescues the impairment related to altered neuromuscular junctions function in the zebrafish transient Pompe disease model.

Translated to PD patients, we can hypothesize that the 3,4-DAPP treatment not only has a beneficial action on already formed NMJs, but can have a therapeutic role even in early NMJs development, hence suggesting a possible higher effect in the early stages of the infantile-onset PD.

Moreover, our results further suggest the inclusion of Pompe disease in the group of pathologies, at least in part characterized by NMJs deterioration, and potentially improved with drugs targeted to the NMJ itself.

Hence, based on our results, we propose 3,4-Diaminopyridine phosphate as symptomatic treatment in infantile- and late-onset Pompe disease patients to improve muscle weakness and fatigability.

The fact that 3,4-DAPP is a drug already approved by Food and Drug Administration (FDA) and by the European Medicines Agency (EMA), will make it easier and accessible to PD patients, improving efficiently the quality of life for themselves and their families.

Declaration of competing interest

None declared.

Acknowledgements

This work was funded by Catalyst Pharmaceuticals Inc, Coral Gables, FL, USA.

We are grateful to Dr. Mora Marina and to Dr. Iyadurai Stanley who have given critical comments on this work. Moreover, Dr. Mora Marina helped in analyzing the data.

Author contributions

Conceived and designed the experiments: **C.B. and G.I.**; performed the experiments: **C.B. and F.B.**; analyzed the data: **C.B.**; wrote the paper: **C.B. and L.M.**; made critical revision of the manuscript for important intellectual content: **C.B., G.I., R.M. and L.M.**

Appendix A. Supporting information

Supplementary data associated with this article can be found in the online version at doi:10.1016/j.biopha.2021.111357.

References

[1] L.R. Chen, C.A. Chen, S.N. Chiu, Y.H. Chien, N.C. Lee, M.T. Lin, W.L. Hwu, J. K. Wang, M.H. Wu, Reversal of cardiac dysfunction after enzyme replacement in patients with infantile-onset Pompe disease, J. Pedia 155 (2009) 271–275, https://doi.org/10.1016/j.jpeds.2009.03.015.

[2] S. Strothotte, N. Strigl-Pill, B. Grunert, C. Kornblum, K. Eger, C. Wessig, M. Deschauer, F. Breunig, F.X. Glocker, S. Vielhaber, A. Brejova, M. Hilz, K. Reiners, W. Müller-Felber, E. Mengel, M. Spranger, B. Schoser, Enzyme replacement therapy with alglucosidase alfa in 44 patients with late- onset glycogen storage disease type 2: 12-month results of an observational clinical trial, J. Neurol. 257 (2010) 91–97, https://doi.org/10.1007/s00415-009-5275-3.

[3] B. Schoser, V. Hill, N. Raben, Therapeutic approaches in glycogen storage disease type II/Pompe disease, Neurotherapeutics 5 (2008) 569–578, https://doi.org/10.1016/j.nurt.2008.08.009.

[4] T.P. Mechtler, S. Stary, T.F. Metz, V.R. De Jesús, S. Greber-Platzer, A. Pollak, K. R. Herkner, B. Streubel, D.C. Kasper, Neonatal screening for lysosomal storage

disorders: feasibility and incidence from a nationwide study in Austria, Lancet 379 (2012) 335–341, https://doi.org/10.1016/S0140-6736(11)61266-X.
[5] N. Raben, M. Danon, A.L. Gilbert, S. Dwivedi, B. Collins, B.L. Thurberg, R. J. Mattaliano, K. Nagaraju, P.H. Plotz, Enzyme replacement therapy in the mouse model of Pompe disease, Mol. Genet. Metab. 80 (2003) 159–169, https://doi.org/10.1016/j.ymgme.2003.08.022.
[6] J.M.P. Van den Hout, J.H.J. Kamphoven, L.P.F. Winkel, W.F.M. Arts, J.B.C. D. Klerk, M.C.B. Loonen, A.G. Vulto, A. Cromme-Dijkhuis, N. Weisglas-Kuperus, W. Hop, H.V. Hirtum, O.P.V. Diggelen, M. Boer, M.A. Kroos, P.A.V. Doorn, E. V. Voort, B. Sibbles, E.J.J.M.V. Corven, J.P.J. Brakenhoff, J.V. Hove, J.A. M. Smeitink, G. Jong, A.J.J. Reuser, A.T.V. Ploeg, Long-term intravenous treatment of Pompe disease with recombinant human alpha-glucosidase from milk, Pediatrics 113 (2004) e448–e457, https://doi.org/10.1542/peds.113.5.e448.
[7] B.L. Thurberg, C. Lynch Maloney, C. Vaccaro, K. Afonso, A.C.H. Tsai, E. Bossen, P. S. Kishnani, M. O'Callaghan, Characterization of pre- and post-treatment pathology after enzyme replacement therapy for Pompe disease, Lab Investig. 86 (2006) 1208–1220, https://doi.org/10.1038/labinvest.3700484.
[8] M. Cardone, C. Porto, A. Tarallo, M. Vicinanza, B. Rossi, E. Polishchuk, F. Donaudy, G. Andria, M. De Matteis, G. Parenti, Abnormal mannose-6-phosphate receptor trafficking impairs recombinant alphaglucosidase uptake in Pompe disease fibroblasts, Pathogenetics 1 (2008), 6, https://doi.org/10.1186/1755-8417-1-6.
[9] A.T. van der Ploeg, A.J. Reuser, Pompe's disease, Lancet 372 (2008) 1342–1353, https://doi.org/10.1016/S0140-6736(08)61555-X.
[10] B. Schoser, Pompe disease: what are we missing? Ann. Transl. Med. 7 (2019), 292 https://doi.org/10.21037/atm.2019.05.29.
[11] M.L.C. Hagemans, S.P.M. Schie, A.C.J.W. Janssens, P.A. Doorn, A.J.J. Reuser, A. T. Ploeg, Fatigue: an important feature of late-onset Pompe disease. J. Neurol. 254 (2007) 941–945, https://doi.org/10.1007/s00415-006-0434-2.
[12] D. Güngör, J.M. de Vries, E. Brusse, M.E. Kruijshaar, W.C.J. Hop, M. Murawska, L. E.M. van den Berg, A.J.J. Reuser, P.A. van Doorn, M.L.C. Hagemans, I. Plug, A. T. van der Ploeg, Enzyme replacement therapy and fatigue in adults with Pompe disease, Mol. Genet. Metab. 109 (2013) 174–178, https://doi.org/10.1016/j.ymgme.2013.03.016.
[13] A.G. Todd, J.A. McElroy, R.W. Grange, D.D. Fuller, G.A. Walter, B.J. Byrne, D. J. Falk, Correcting neuromuscular deficits with gene therapy in Pompe disease, Ann. Neurol. 78 (2015) 222–234, https://doi.org/10.1002/ana.24433.
[14] D.J. Falk, A.G. Todd, S. Lee, M.S. Soustek, M.K. ElMallah, D.D. Fuller, L. Notterpek, B.J. Byrne, Peripheral nerve and neuromuscular junction pathology in Pompe disease, Hum. Mol. Genet. 24 (2015) 625–636, https://doi.org/10.1093/hmg/ddu476.
[15] C. Bragato, S. Carra, F. Blasevich, F. Salerno, A. Brix, A. Bassi, M. Beltrame, F. Cotelli, L. Maggi, R. Mantegazza, M. Mora, Glycogen storage in a zebrafish Pompe disease model is reduced by 3-BrPA treatment, Biochim. Biophys. Acta Mol. Basis Dis. 1866 (5) (2020), 165662, https://doi.org/10.1016/j.bbadis.2020.165662.
[16] P. Wirtz, J. Verschuuren, J. van Dijk, M. de Kam, R. Schoemaker, J. van Hasselt, M. Titulaer, U. Tjaden, J. den Hartigh, J. van Gerven, Efficacy of 3,4-diaminopyridine and pyridostigmine in the treatment of Lambert-Eaton myasthenic syndrome: a randomized, double-blind, placebo-controlled, crossover study, Clin. Pharmacol. Ther. 86 (2009) 44–48, https://doi.org/10.1038/clpt.2009.35.
[17] H. Lundh, O. Nilsson, I. Rosen, Treatment of Lambert-Eaton syndrome: 3,4-diaminopyridine and pyridostigmine, Neurology 34 (1984) 1324–1330, https://doi.org/10.1212/wnl.34.10.1324.
[18] D.B. Sanders, V.C. Juel, Y. Harati, A.G. Smith, A.C. Peltier, T. Marburger, J.S. Lou, R.M. Pascuzzi, D.P. Richman, T. Xie, V. Demmel, L.R. Jacobus, K.L. Aleš, D. P. Jacobus, 3,4-diaminopyridine base effectively treats the weakness of Lambert-Eaton myasthenia, Muscle Nerve 57 (2018) 561–568, https://doi.org/10.1002/mus.26052.
[19] R.H. Thomsen, D.F. Wilson, Effects of 4-aminopyridine and 3,4-diaminopyridine on transmitter release at the neuromuscular junction, J. Pharmacol. Exp. Ther. 227 (1) (1983) 260–265.
[20] N. Ishida, Y. Kondo, Y. Chikano, E. Kobayashi-Nakade, Y. Suga, J. Ishizaki, K. Komai, R. Matsushita, Pharmacokinetics and tissue distribution of 3,4-diaminopyridine in rats, Biopharm. Drug Dispos. 40 (2019) 294–301, https://doi.org/10.1002/bdd.2203.
[21] S.A. Raffertya, T.A. Quinn, A beginner's guide to understanding and implementing the genetic modification of zebrafish, Prog. Biophys. Mol. Biol. 138 (2018) 3–19, https://doi.org/10.1016/j.pbiomolbio.2018.07.005.
[22] S. Saleem, R.R. Kannan, Zebrafish: an emerging real-time model system to study Alzheimer's disease and neurospecific drug discovery, Cell Death Discov. 4 (2018), 45, https://doi.org/10.1038/s41420-018-0109-7.
[23] C.B. Kimmel, W.W. Ballard, S.R. Kimmel, B. Ullmann, T.F. Schilling, Stages of embryonic development of the zebrafish, Dev. Dyn. 203 (1995) 253–310, https://doi.org/10.1002/aja.1002030302.
[24] A. Nasevicius, S.C. Ekker, Effective targeted gene 'knockdown' in zebrafish, Nat. Genet. 26 (2000) 216–220, https://doi.org/10.1038/79951.
[25] J. Schindelin, I. Arganda-Carreras, E. Frise, V. Kaynig, M. Longair, T. Pietzsch, S. Preibisch, C. Rueden, S. Saalfeld, B. Schmid, J.Y. Tinevez, D.J. White, V. Hartenstein, K. Eliceiri, P. Tomancak, A. Cardona, Fiji: an open-source platform for biological-image analysis, Nat. Methods 9 (7) (2012) 676–682, https://doi.org/10.1038/nmeth.2019.
[26] J.J. Dowling, A.P. Vreede, S.E. Low, E.M. Gibbs, J.Y. Kuwada, C.G. Bonnemann, E. L. Feldman, Loss of myotubularin function results in T-tubule disorganization in zebrafish and human myotubular myopathy, PLoS Genet. 5 (2) (2009), e1000372, https://doi.org/10.1371/journal.pgen.1000372.
[27] H.J. Tsay, Y.H. Wang, W.L. Chen, M.Y. Huang, Y.H. Chen, Treatment with sodium benzoate leads to malformation of zebrafish larvae, Neurotoxicol. Teratol. 29 (2007) 562–569, https://doi.org/10.1016/j.ntt.2007.05.001.
[28] L. Benedetti, A. Ghilardi, E. Rottoli, M. De Maglie, L. Prosperi, C. Perego, M. Baruscotti, A. Bucchi, L. Del Giacco, M. Francolini, INaP selective inhibition reverts precocious inter- and motorneurons hyperexcitability in the Sod1-G93R zebrafish ALS model, Sci. Rep. 6 (2016), 24515, https://doi.org/10.1038/srep24515.
[29] M. Granato, F.J. van Eeden, U. Schach, et al., Genes controlling and mediating locomotion behavior of the zebrafish embryo and larva, Development 123 (1996) 399–413.
[30] C. Bragato, G. Gaudenzi, F. Blasevich, G. Pavesi, L. Maggi, M. Giunta, F. Cotelli, M. Mora, Zebrafish as a model to investigate Dynamin-2-related diseases, Sci. Rep. 6 (2016), 20466, https://doi.org/10.1038/srep20466.
[31] S. Bolte, F.P. Cordelières, A guided tour into subcellular colocalization analysis in light microscopy, J. Microsc. 224 (2006) 213–232, https://doi.org/10.1111/j.1365-2818.2006.01706.x.
[32] S. Pushpakom, F. Iorio, P.A. Eyers, K.J. Escott, S. Hopper, A. Wells, A. Doig, T. Guilliams, J. Latimer, C. McNamee, A. Norris, P. Sanseau, D. Cavalla, M. Pirmohamed, Drug repurposing: progress, challenges and recommendations, Nat. Rev. Drug Discov. 18 (2019) 41–58, https://doi.org/10.1038/nrd.2018.168.
[33] S. Bonanno, M.B. Pasanisi, R. Frangiamore, L. Maggi, C. Antozzi, F. Andreetta, A. Campanella, G. Brenna, L. Cottini, R. Mantegazza, Amifampridine phosphate in the treatment of muscle-specific kinase myasthenia gravis: a phase IIb, randomized, double-blind, placebo-controlled, double crossover study, SAGE Open Med. 6 (2018), 205031211881901, https://doi.org/10.1177/2050312118819013.
[34] R. Mantegazza, A. Meisel, J.P. Sieb, G. Le Masson, C. Desnuelle, M. Essing, The European LEMS registry: baseline demographics and treatment approaches, Neurol. Ther. 4 (2) (2015) 105–124, https://doi.org/10.1007/s40120-015-0034-0.
[35] L. Maggi, P. Bernasconi, A. D'Amico, R. Brugnoni, C. Fiorillo, M. Garibaldi, G. Astrea, C. Bruno, F.M. Santorelli, R. Liguori, G. Antonini, A. Evoli, E. Bertini, C. Rodolico, R. Mantegazza, Italian recommendations for diagnosis and management of congenital myasthenic syndromes, Neurol. Sci. 40 (2019) 457–468, https://doi.org/10.1007/s10072-018-3682-x.
[36] T. Fukuda, A. Roberts, M. Ahearn, K. Zaal, E. Ralston, P.H. Plotz, N. Raben, Autophagy and lysosomes in Pompe disease, Autophagy 2 (2006) 318–320, https://doi.org/10.4161/auto.2984.
[37] F. Zindler, F. Beedgen, D. Brandt, M. Steiner, D. Stengel, L. Baumann, T. Braunbeck, Analysis of tail coiling activity of zebrafish (Danio rerio) embryos allows for the differentiation of neurotoxicants with different modes of action, Ecotoxicol. Environ. Saf. 186 (2019), 109754, https://doi.org/10.1016/j.